Available online at www.sciencedirect.com
ScienceDirect
Applied Mathematics and Computation 184 (2007) 73–85
APPLIED MATHEMATICS AND COMPUTATION
www.elsevier.com/locate/amc

A two-dimensional thin-film transistor simulation using adaptive computing technique

Yiming Li

Department of Communication Engineering, National Chiao Tung University, 1001 Ta-Hsueh Road, Hsinchu 300, Taiwan

Abstract

In this paper, an adaptive computational technique is applied to solve a set of two-dimensional (2D) drift-diffusion (DD) equations together with nonlinear trap model in thin-film transistors (TFTs). Different from the conventional DD equations in metal-oxide-semiconductor field effect transistors, the nonlinear trap model depending on the potential energy accounts for the effect of grain boundary on the electrical characteristics of low temperature polycrystalline-silicon (LTPS) TFTs. Our adaptive computing technique is mainly based on Gummel's decoupling method, a finite volume (FV) approximation, a monotone iterative (MI) method, a posteriori error estimation, and an 1-irregular meshing scheme. Applying Gummel's decoupling method to the set of DD equations firstly, each decoupled partial differential equation (PDE) is then approximated with FV method over 1-irregular mesh. Instead of conventional Newton's iterative method, the corresponding system of nonlinear algebraic equations is solved with MI method. Variations of the computed solutions, such as potential and electron density are captured and a posteriori error estimation scheme is adopted to assess the quality of the computed solutions. The mesh is adaptively refined accordingly. The numerical method converges monotonically in both MI and Gummel's iteration loops, respectively. Various cases of simulation have been verified for a typical LTPS TFT to demonstrate the accuracy and robustness of the method.

Keywords: Adaptive computing; Monotone iterative method; Drift-diffusion equations; Nonlinear trap model; Grain boundary; Thin-film transistor; Semiconductor device simulation

1. Introduction

Development of low temperature polycrystalline-silicon (LTPS) thin-film transistors (TFTs) has recently been of great interest in micro- and opto-electronics industries; in particular, for the industry of display panel [1–6]. Modeling and simulation of semiconductor devices theoretically provide alternative way to the interpretation of experimental results [7–9]. It is known that a set of drift-diffusion (DD) equations consisting of the Poisson equation, the current continuity equation of electron, and the current continuity equation of hole

E-mail address: ymli@faculty.nctu.edu.tw

0096-3003/$ - see front matter
doi:10.1016/j.amc.2005.12.073

has successfully been applied to explore transport phenomena of electron and hole in semiconductor devices [1,7–9]. Compared with conventional metal-oxide-semiconductor field effect transistors (MOSFETs), LTPS TFTs possess significant grain structures in the silicon substrate of TFT shown in Figs. 1 and 2. They then produce different impurity traps, and affect the charge distribution as well as transport properties [1–6,10,11]. Therefore, it is necessary to accurately describe grain structures and calculate the effect of grain boundary on the electrical characteristics when performing technology computer-aided design (TCAD) tools. However, numerical solution of DD equations together with the nonlinear trap model of LTPS TFTs may encounter convergence problem due to the equations to be solved is highly nonlinear dependence on the potential energy.

In this paper, a physical-based nonlinear trap model is introduced which describes the effect of grain topologies on the intrinsic physical quantities, such as potential energy and electron density for LTPS TFTs. The nonlinear trap model is solved together with Poisson equation in a set of the two-dimensional (2D) DD equations. In the numerical solution of nonlinear-trap corrected DD equations for LTPS TFTs, a computationally cost-effective adaptive computing technique is implemented [12–17]. First of all we decouple the three partial differential equations (PDEs) in the set of DD equations according to Gummel's procedure [18,19]. Based on adaptive 1-irregular mesh [20,21] and finite volume (FV) approximation [12–17,22,23], each decoupled PDE is discretized and then solved by means of the monotone iterative (MI) method [24–26] instead of Newton's iteration (NI) method [27]. The method of monotone iteration is a constructive alternative for numerical solutions of PDEs [25,26]. It has been reported that, compared with NI method, the major features of MI method are (1) it converges globally with any arbitrary initial guesses; (2) its implementation is much easier than NI method; and (3) it is inherently ready for parallelization [24]. Furthermore, using a posteriori error estimation, the gain boundary induced variation of physical quantities, such as electric field and gradient of electron density, are accurately calculated and automatically tracked. We note that the adaptive computing technique was successfully developed in our recent work for various MOSFETs simulation [3,12–17]. Testing on different LTPS TFTs, the proposed adaptive computing technique shows the simulation accuracy and numerical robustness. Achieved result shows that our computational approach provides a cost-effective way to solve a set of DD equations with the nonlinear trap model of grain boundary for advanced LTPS TFTs' simulation.

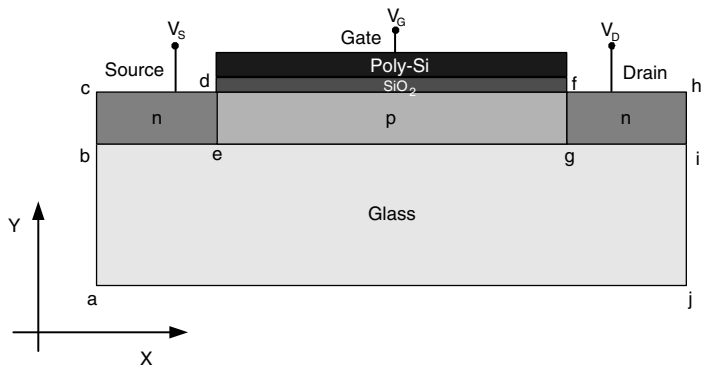

Fig. 1. A cross-section view of the simulated LTPS TFT.

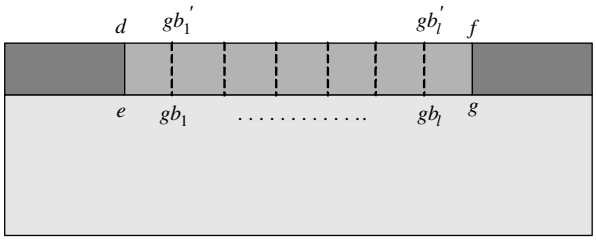

Fig. 2. An illustration of the cross-section view and boundary conditions of grains.

This paper is organized as follows. In the Section 2, we introduce the studied transport model for the numerical simulation of LTPS TFTs. In the Section 3, we state the adaptive computing technique. In the Section 4, we report and discuss the results of numerical simulation. In the Section 5, we draw the conclusions.

2. A set of DD equations for LTPS TFTs

In this section, we state a 2D mathematical model of DD equations together with the nonlinear trap model for LTPS TFTs, shown in Fig. 1. It is known that classical DD equations consist of three coupled PDEs, the Poisson equation, the current continuity equation of electron, and the current continuity equation of hole [1,7–9]. By considering the nature of Poly-Si induced grain boundaries [1–6,10,11] in the structure of LTPS TFTs, a set of 2D DD equations is give by

$$\Delta\phi = \frac{q}{\varepsilon_s}(n - p + D(x,y) + BT(\phi)), \tag{1}$$

$$BT(\phi) = N_{At} f_{p0} \exp\left(-\frac{\phi - \phi_E}{V_T}\right), \tag{2}$$

$$\frac{1}{q}\nabla\cdot(-q\mu_n n\nabla\phi + qD_n\nabla n) = R(n,p), \tag{3}$$

and

$$\frac{1}{q}\nabla\cdot(-q\mu_p p\nabla\phi + qD_p\nabla p) = -R(n,p). \tag{4}$$

Eq. (1) is the so-called Poisson equation, where the unknown $\phi = \phi(x,y)$ to be solved in the domain, shown in Fig. 1, is the electrostatic potential. Eqs. (3) and (4) are the current continuity equations of electron and hole, respectively, where the unknowns n and p to be solved are the densities of electron and hole. In Eq. (1), q is the elementary charge, ε_s is the silicon permittivity, and $D(x, y)$ is the spatial-dependent doping profile [1]. Eq. (2) is a distribution function of the grain boundary which occurs on the grain boundaries $\overline{gb_i gb_i'}$, $i = 1, \ldots, l$, where l is the number of grain boundaries, shown in Fig. 2. $BT(\phi)$ in Eq. (2) is a nonlinear equation of electrostatic potential ϕ and is solved together with the Poisson equation in Eq. (1). N_{At} is the concentration of acceptor trap and $f_{p0}\exp\left(-\frac{\phi-\phi_E}{V_T}\right)$ is the occupation probabilities of hole. ϕ_E is assumed to be the periodical energy band structure along the conducting channel in the neighborhood of the grain boundaries. f_{p0} is an initial probability of hole. μ_n and μ_p in Eqs. (3) and (4) are the mobilities of electron and hole. D_n and D_p are the diffusion coefficients of electron and hole, and $R(n, p)$ is the term of generation-recombination of electron and hole [1].

Eqs. (1)–(4) are subject to proper boundary conditions for ϕ, n, and p [1,7–9,13], shown in Fig. 1. The boundaries $\overline{cd}$, $\overline{fh}$, and $\overline{aj}$ are specified by the type of Dirichlet boundary condition for ϕ, n, and p, respectively. In order to guarantee that the simulated LTPS TFT is self contained, the boundaries $\overline{ac}$ and $\overline{hj}$ are assumed to be the homogeneous Neumann boundary condition for ϕ, n, and p, respectively. On the interfaces of Si and SiO_2, the boundaries $\overline{df}$ and $\overline{eg}$, Gauss's law in differential form must be obeyed for ϕ. For the current continuity equations of electron and hole, we assume that the Si_2 and glass are perfect insulators, and that the surface recombination rate is zero. Under these circumstances, the normal components of the electron and hole currents vanish on the interfaces, the boundaries $\overline{df}$ and $\overline{eg}$. It results in the homogeneous Neumann boundary condition for n and p.

3. Adaptive computing technique

The implemented adaptive computing technique for LTPS TFT simulation is mainly based on Gummel's decoupling method [7–9,18,19], FV approximation [9,13–17,24,27], MI method [24–26], a posteriori error estimation [13], and an 1-irregular meshing scheme [12–15]. This simulation methodology has recently been developed for different MOSFET's simulation [3,12–17]. To explore the transport behavior of LTPS TFTs, the three coupled PDEs are numerically solved with Gummel's decoupling method. With a given initial guess

$(\phi^{(0)}, n^{(0)}, p^{(0)})$ and for each Gummel's iteration index g, $g = 0, 1, \ldots$, we first solve the nonlinear Poisson equation

$$\Delta\phi^{(g+1)} = \frac{q}{\varepsilon_s}(n^{(g)} - p^{(g)} + D(x,y) + BT(\phi^{(g+1)})). \tag{5}$$

The nonlinear Poisson equation is solved for $\phi^{(g+1)}$ given the previous states $n^{(g)}$ and $p^{(g)}$. The current continuity equation of electron is then solved for $n^{(g+1)}$, with now the known functions $\phi^{(g+1)}$ and $p^{(g)}$

$$\frac{1}{q}\nabla\cdot(-q\mu_n n^{(g+1)}\nabla\phi^{(g)} + qD_n^{(g+1)}\nabla_n^{(g+1)}) = R(n^{(g+1)}, p^{(g)}). \tag{6}$$

Finally, we solve the current continuity equation of hole with both $\phi^{(g+1)}$ and $n^{(g+1)}$ known

$$\frac{1}{q}\nabla\cdot(-q\mu_p p^{(g+1)}\nabla\phi^{(g+1)} + qD_p^{(g+1)}\nabla_p^{(g+1)}) = -R(n^{(g+1)}, p^{(g+1)}) \tag{7}$$

for $p^{(g+1)}$ until all preset stopping criteria are satisfied. Eqs. (5)–(7) are associated with proper boundary condition, respectively. We note that Eqs. (5)–(7) are now three individual semilinear PDEs to be solved for each Gummel's iteration. An outer iteration in the procedure of LTPS TFT simulation is then defined by Gummel's decoupling method. We note that analyses of Gummel's decoupling method in MOSFET simulation have been reported [7,8,19].

```
The Gummel's decoupling method
Begin
  While φ, n, and p in outer loop (Gummel's loop) are not convergent
    If φ is convergent
      Solve the nonlinear Poisson equation
      with adaptive computing technique.
    End If
    If n is convergent
      Solve the current continuity equation of electron
      with adaptive computing technique.
    End If
    If p is convergent
      Solve the current continuity equation of hole
      with adaptive computing technique.
    End If
  End While
  Call for next calculation.
End The Gummel's decoupling algorithm
```

A computational procedure for Gummel's decoupling method is shown above, where we solve each decoupled PDE with adaptive computing technique. In the adaptive computing technique, each PDE is approximated with FV method over 1-irregular mesh. The corresponding system of nonlinear algebraic equations of FV discretization of PDE is solved with MI method. In error estimation and mesh refinement, a posteriori error estimation scheme is applied to assess the quality of computed solutions. The adaptive mechanism bases on an estimation of the variation of computed solutions, such as the electric field, the gradient of electron density, and the lateral current density. A posteriori error estimation is applied to provide local error indicators for incorporation into the mesh refinement strategy. The local error indicators guide the adaptive refinement process.

For each PDE, shown in Eqs. (5)–(7), by directly considering a problem of semilinear elliptic PDE, we briefly state a MI method for the numerical solution of the boundary value problem. Over a ceratin partition of simulation domain, applying the adopted discretization method, the finite volume approximation to the explored semilinear elliptic PDE together with its mixed-type boundary condition, we obtain a system of nonlinear algebraic equations in a compact form

$$AZ = -F(Z), \tag{8}$$

where A is an $M \times M$ matrix, $Z \equiv (w_1, \ldots, w_M)^{\mathrm{T}}$ is an unknown vector, and $F(Z) \equiv (F_1(Z), \ldots, F_M(Z))^{\mathrm{T}}$ is a vector associated with the functions appearing in the right hand side of PDE and boundary condition. It is sufficient to consider a specified solution method for solving the system of nonlinear algebraic equations. Starting with a given initial vector $Z^{(0)}$ for Eq. (8), MI method generates a sequence of iterates $\{Z^{(n)}\}$, $n = 0, 1, \ldots$, by solving

$$AZ^{(n+1)} + \Lambda Z^{(n+1)} = -F(Z^{(n)}) + \Lambda Z^{(n)}, \tag{9}$$

where Λ is a nonnegative diagonal matrix in which its entries λ_{kk}, $k = 1, \ldots, M$, are parameters that are determined principally by the property of nonlinear function in the right hand side of PDE. Under various conditions on the matrices A and Λ, or equivalently on the discretization and the nonlinear function in the right hand side of PDE, it is known that the sequence $\{Z^{(n)}\}$ generated by Eq. (9) converges monotonically to a solution of (8). Obviously, the convergence behavior of MI process (9) is essentially dictated by these parameters. There are some variants of MI form (9), such as Jacobi, Seidel, and block MI methods [26]. For LTPS TFTs simulation, we use in particular the Jacobi method

$$(D + \Lambda)Z^{(n+1)} = (L + U)Z^{(n)} - F(Z^{(n)}) + \Lambda Z^{(n)} \tag{10}$$

where D, L, and U are diagonal, lower triangular, and upper triangular matrices of A, respectively. The essence and convergence of the monotone iterative method for the numerical solution of PDE in MOSFET simulation has been studied in our recent work [24].

Once an approximated solution is computed, we perform a posteriori error analysis to assess its quality, and the error analysis produces error indicators and an error estimator. If the estimator is less than a specified error tolerance (TOL), the adaptive process will be terminated and the approximated solution can be output for post-process and analysis. Otherwise, we employ a scheme to refine current elements depending on the magnitude of the error indicator. A finer partition of the domain is thus created, and a new solution procedure is repeated iteratively. We note that for FV approximation, control volumes have to select with respect to their dual elements. According to our classification, different pattern of boundary of control volume in the reference element is identified by verifying the number and location of irregular nodes appearing in that element [13]. A computational procedure of the adaptive computing technique is summarized as follows.

```
The adaptive computing technique for decoupled PDE
Begin
  Let a decoupled PDE and a specified error tolerance (TOL) are given;
  Perform discretization of the simulation domain;
  Perform FV approximation;
  Construct the system of nonlinear algebraic Eq. (8);
  Solve the nonlinear system with MI method by Eq. (10);
  Compute the maximum error (Err) of the computed solution;
  If Err > TOL
    Run 1-irregular mesh refinement and
    Go to the step of domain discretization and repeat the steps,
  Else
    Post-process.
  End If
End The adaptive computing technique
```

4. Results and discussion

We now present numerical results to demonstrate effect of the proposed physical model and performance of the adaptive computing technique in LTPS TFT simulation. As shown in Fig. 1, the simulated TFT device is

with $\overline{aj} = 4$ μm, $\overline{be} = \overline{gi} = 1$ μm, and $\overline{ac} = \overline{hj} = 0.5$ μm. The gate oxide thickness of the S_iO_2 layer is equal to 10 nm. The junction depth is with $\overline{bc} = \overline{hi} = 0.05$ μm. The channel length $\overline{df} = \overline{eg} = 2$ μm. The 0.2 μm grain size is considered in this work [10,11]. Hence, there are ten grain boundaries along the direction of channel. The LTPS TFT is assumed to have an elliptical-shaped Gaussian doping profile, where the peak concentration is equal to 2×10^{20} cm^{-3}. Fig. 3 shows the used spatial-dependent doping profile $D(y, x)$ in the LTPS TFT simulation.

Figs. 4–6 show the process of mesh refinements in a MI loop. The mechanism of 1-irregular mesh refinement is based on the estimation of solution error element by element. Fig. 4 is the initial mesh which contains 25 nodes, Fig. 5 is the 4th refined mesh containing 729 nodes, and Fig. 6 contains 3868 nodes is the 7th mesh. We note that the process of mesh refinement is guided by the result of error estimation automatically. As shown in Fig. 6, at the 7th refined level we find that most of refined meshes are intensively located near the surface of channel and the junction of the drain side due to large variation of the solution gradient. The distribution of refined mesh is consistent with the profile of computed electrostatic potential, shown in Fig. 7.

The number of nodes (and elements) versus the number of levels of mesh refinement is shown in Fig. 8. The simulations are with and without including the nonlinear trap model to account for the effect of grain boundary. The number of refined elements and nodes is increased as the refinement levels are increased. At the beginning, the number of refined nodes (and elements) is increased fast due to significant variations of computed solution. After several refinements and solution processes, the increasing rate of the number of nodes (and elements) gradually becomes slow when the refinements are increased. It eventually reaches to a saturated condition.

Figs. 9 and 10 show the convergence behavior of Gummel's (outer) and MI (inner) loops when solving the electrostatic potential with (w/) and without (w/o) including the trap model of grain boundary in the simulated TFT device. Here, we also defined an additional linear trap model of grain boundary by setting $BT(\phi) = N_{At}$.

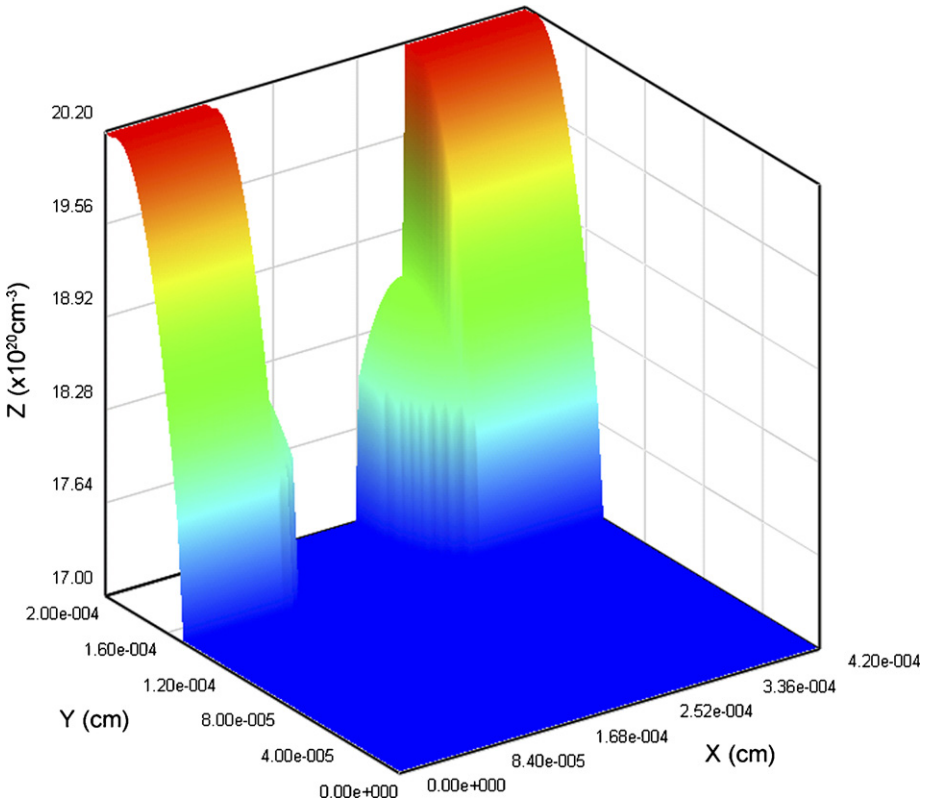

Fig. 3. An illustration of the doping profile used in the numerical simulation of LTPS TFTs.

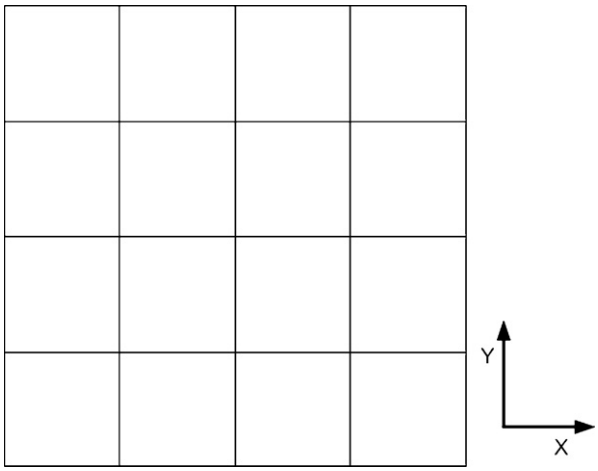

Fig. 4. The initial mesh used for starting the solution process. It contains 25 nodes.

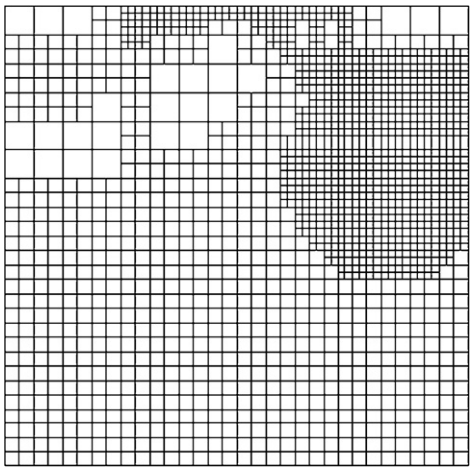

Fig. 5. The 4th refined 1-irregular mesh which contains 729 nodes.

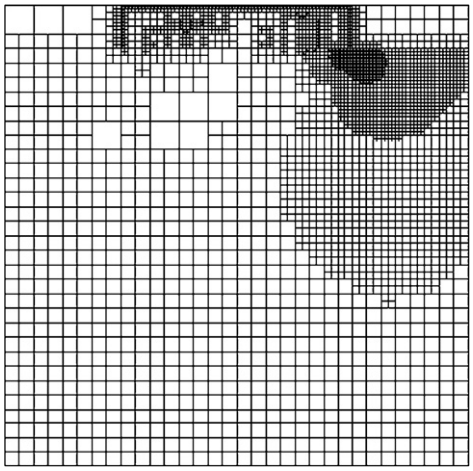

Fig. 6. The 7th refined mesh which contains 3868 nodes.

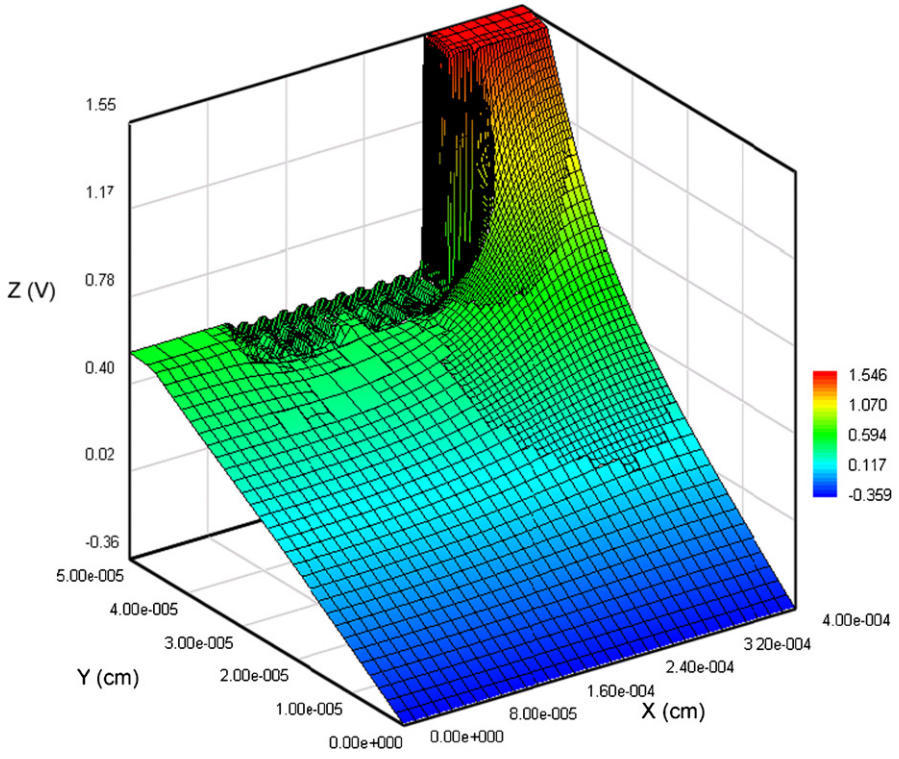

Fig. 7. The simulated electrostatic potential at the 7th level. The LTPS TFT is biased at $V_D = V_G = 1.0$ V.

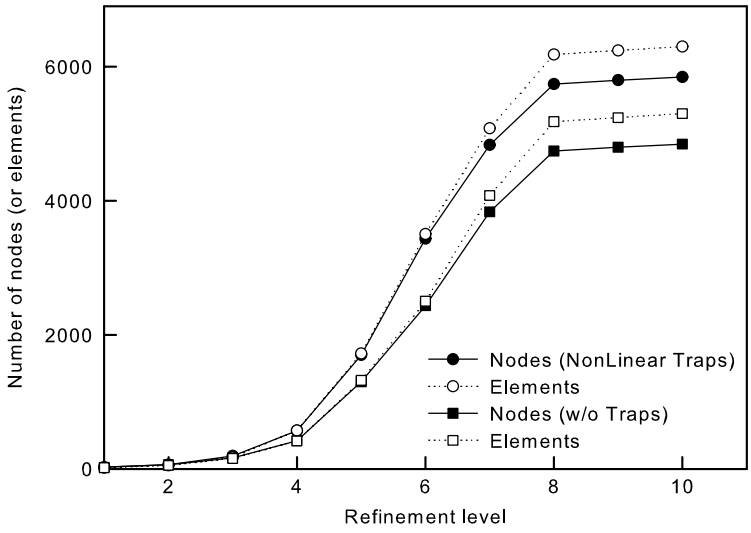

Fig. 8. The number of nodes and elements versus the refinement levels with and without considering the trap models of grain boundary.

The biasing conditions in all simulation cases are $V_D = 1.0$ V and $V_G = 1.0$ V. The stopping criteria for the inner and outer iteration loops are 1e−6 and 1e−3, respectively, for all computed physical quantities. We found that the case of DD simulation without considering any trap models of grain boundary converges quickly among three testing cases. However, the cases of DD simulation with the linear and nonlinear trap models of grain boundary have a similar convergence behavior.

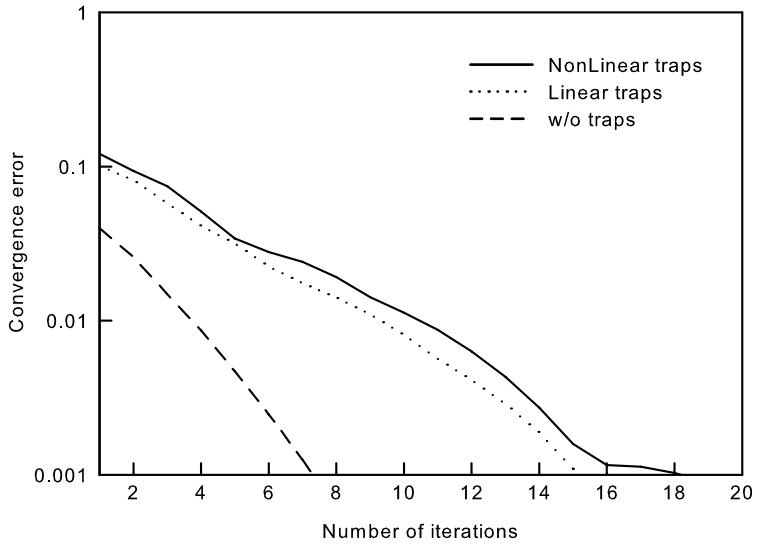

Fig. 9. A convergence property of Gummel's loop for the numerical solution of DD equations with and without including the trap models of grain boundary, where $V_D = V_G = 1.0$ V.

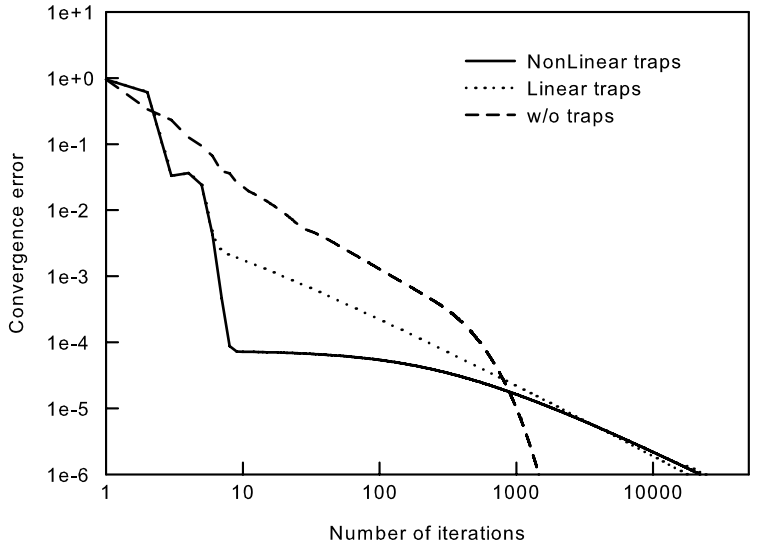

Fig. 10. A convergence behavior of MI loop for the numerical solution of Poisson equation in the set of DD equations with and without including the trap models of grain boundary, where $V_D = V_G = 1.0$ V.

To explore the effect of grain boundary on the physical characteristics of simulated LTPS TFT, we examine the computed electrostatic potential and electron density along the channel direction (x direction) shown in Figs. 11 and 12, respectively. The upper figure of Fig. 11 shows the computed potential profile for the device under bias conditions $V_D = 0.5$ V and $V_G = 0.5$ V, and the lower one in Fig. 11 is a cross-sectional view of the circled region in the upper figure. The upper figure of Fig. 12 shows the electron density and the lower one in Fig. 12 is a cross-sectional view of the circled region in the upper figure. Along the channel region of the device, obviously, the simulated potential profile and electron density significantly reveal the effect of grain boundary on the computed physical quantities.

As shown in Fig. 13, we compare the computed electrostatic potential with different trap models of grain boundary at $V_D = V_G = 0.5$ V. The case of DD simulation with the nonlinear trap model of grain boundary

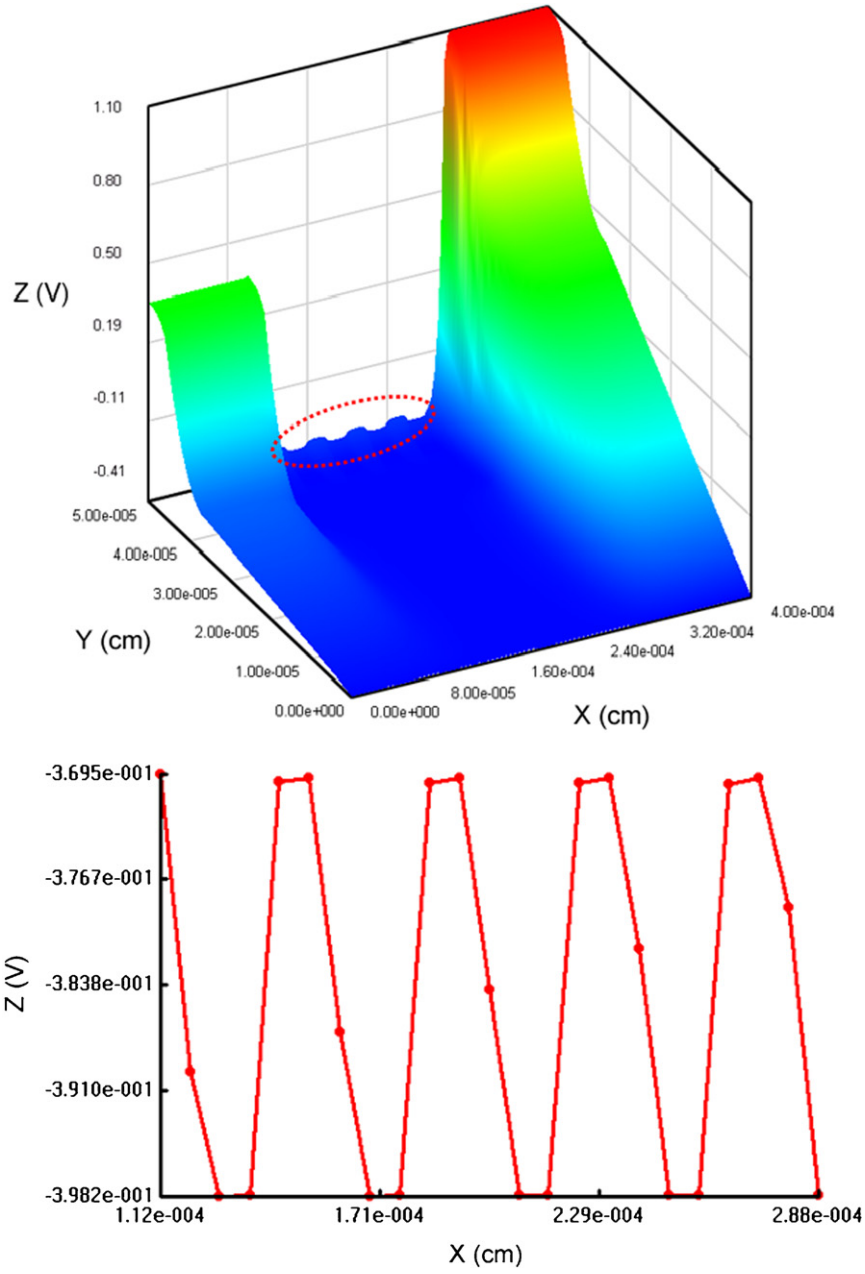

Fig. 11. The upper figure is the simulated potential of the LTPS TFT with $V_D = V_G = 0.5$ V. The lower one is a cross-sectional view of the circled region in the upper figure.

faithfully describes the traps effect on the charge distribution compared with DD simulation including only the linear trap model. The case of DD simulation without including any trap models does not reflect the effect of grain boundary on the computed potential. We further compute the terminal characteristics of current–voltage (I–V) for the investigated LTPS TFT. As shown in Fig. 14, it indicates the difference of the I–V characteristics among DD simulation with the linear trap model of grain boundary, with the nonlinear trap model of grain boundary, and without any trap models. Due to larger variation of the electron density along the channel of TFT, DD simulation together with the nonlinear trap model of grain boundary produces largest current level among three cases.

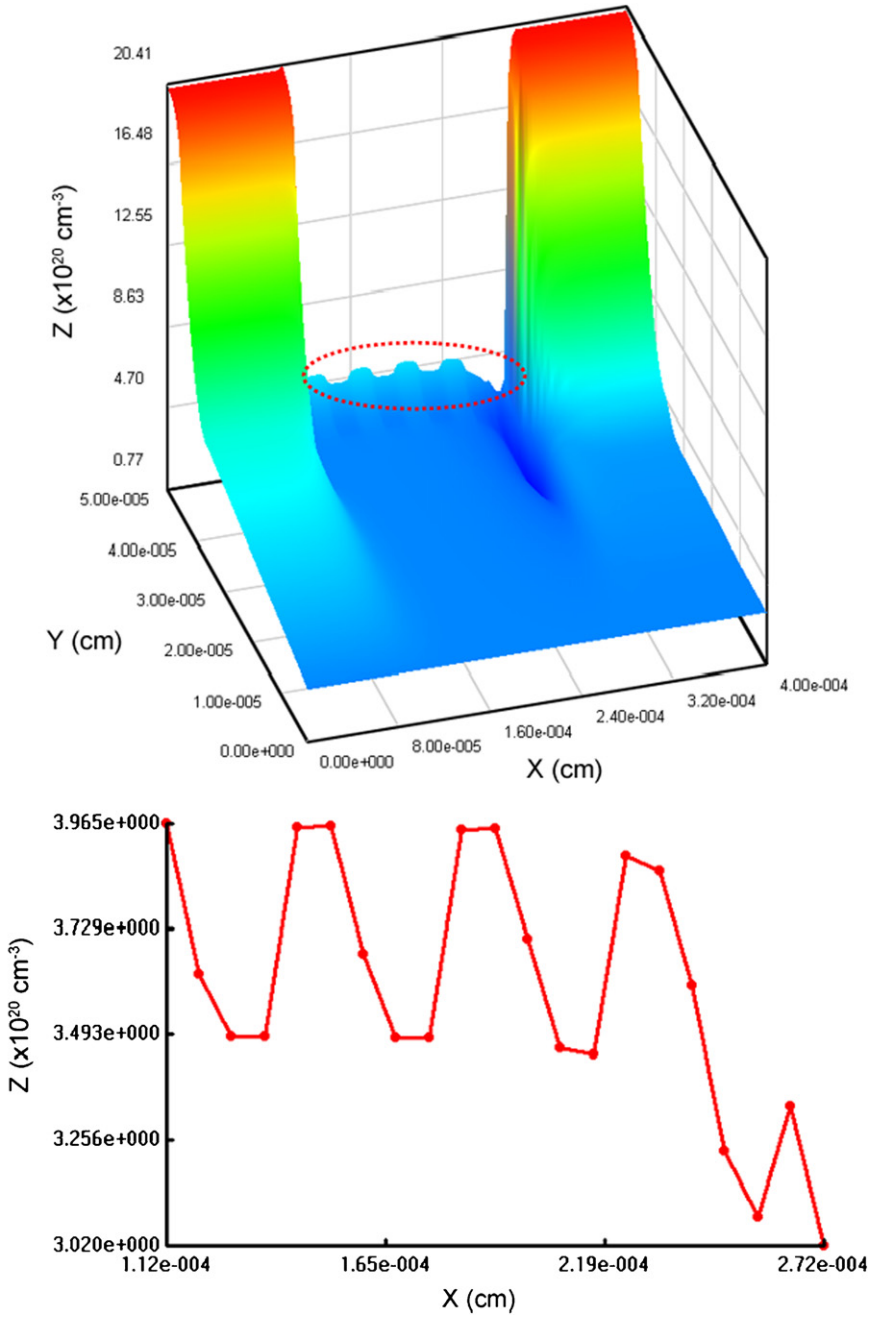

Fig. 12. The upper figure is the simulated electron density of the LTPS TFT with $V_D = V_G = 0.5$ V. The lower one is a cross-sectional view of the circled region in the upper figure.

5. Conclusions

In this paper, we have successfully applied the adaptive computing technique to the 2D simulation of LTPS TFTs. The implemented solution methodology mainly relies on Gummel's decoupling method, the adaptive finite volume method on the 1-irregular mesh, and the monotone iterative method. A nonlinear trap model has been introduced in the set of 2D DD equations to describe the effect of grain boundary on the electrical

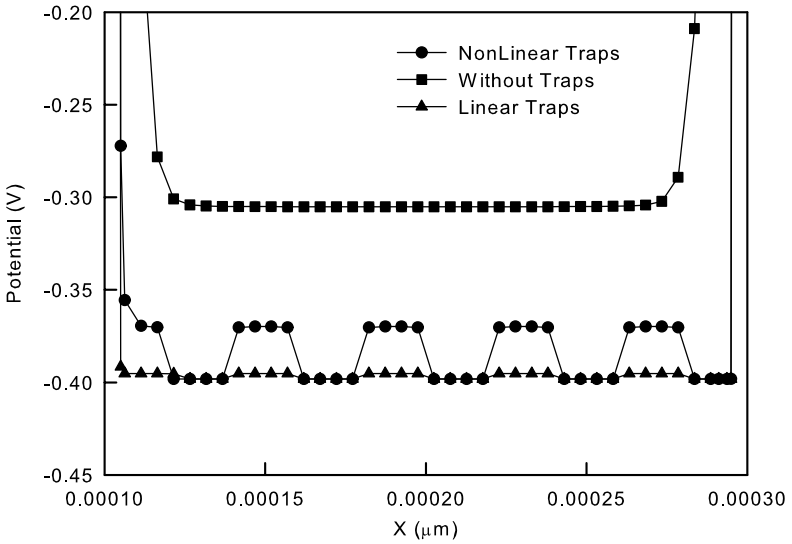

Fig. 13. Comparison of the computed electrostatic potential for the 2D DD simulation with three different trap models of grain boundary, where $V_D = V_G = 0.5$ V.

characteristics of LTPS TFT. Computed physical quantities, such as potential distribution and electron density, and drain current have demonstrated the effect of traps on the device properties. We have computationally found significant difference on the device performance for the LTPS TFT with and without grain traps. Obtained simulations between the refined mesh and the computed potential have demonstrated very good consistency of adaptivity for the testing cases. Convergence and benchmark examinations have been reported to show the robustness and efficiency of the adaptive computing technique for a typical LTPS TFT. We believe the modeling and simulation presented here may benefit the development of TCAD tools for LTPS TFT device simulation in modern industry of display panel.

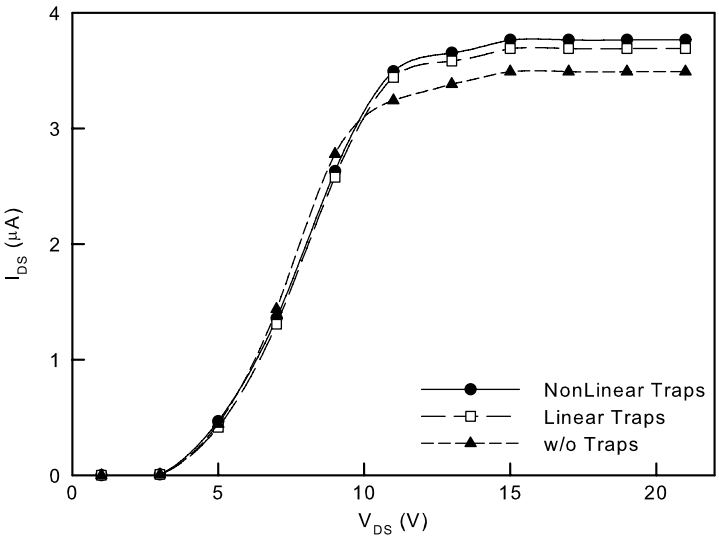

Fig. 14. Comparison of the calculated I–V curves for the studied LTPS TFT with the 2D DD simulation with three different trap models of grain boundary, where $V_G = 1.0$ V.

Acknowledgement

This work was supported in part by the National Science Council (NSC) of TAIWAN under Contract NSC-94-2215-E-009-084 and Contract NSC-95-2752-E-009-003-PAE, and by the MoE ATU Program under a 2006 grant.

References

[1] S.M. Sze, Physics of Semiconductor Devices, second ed., Wiley-Interscience, New York, 1981.
[2] Y. Li, S.-M. Yu, A Novel Approach to Compact Model Parameter Extraction for Excimer Laser Annealed Complementary Thin Film Transistors, Journal of Computational Electronics 3 (2004) 257–261.
[3] Y. Li, Application of Parallel Adaptive Computing Technique to Polysilicon Thin-Film Transistor Simulation, Lecture Notes in Computer Science, LNCS 3726 (2005) 829–838.
[4] A. Bolognesi, M. Berliocchi, M. Manenti, A. Di Carlo, P. Lugli, K. Lmimouni, C. Dufour, Effects of grain boundaries, field-dependent mobility, and interface trap states on the electrical characteristics of pentacene TFT, IEEE Transactions on Electron Devices 51 (2004) 1997–2003.
[5] P.M. Walker, H. Mizuta, S. Uno, Y. Furuta, D.G. Hasko, Improved off-current and subthreshold slope in aggressively scaled poly-Si TFTs with a single grain boundary in the channel, IEEE Transactions on Electron Devices 51 (2004) 212–219.
[6] S. Jagar, C.F. Cheng, S. Zhang, H. Wang, M.C. Poon, C.W. Kok, M. Chan, A SPICE model for thin-film transistors fabricated on grain-enhanced polysilicon film, IEEE Transactions on Electron Devices 50 (2003) 1103–1108.
[7] P.A. Markowich, C.A. Ringhofer, C. Schmeiser, Semiconductor Equations, Springer, Vienna, 1990.
[8] J.W. Jerome, Analysis of Charge Transport: A Mathematical Study of Semiconductor Devices, Springer-Verlag, New York, 1996.
[9] S. Selberherr, Analysis and Simulation of Semiconductor Devices, Springer-Verlag, New York, 1984.
[10] T. Mizuki, J.S. Matsuda, Y. Nakamura, J. Takagi, T. Yoshida, Large domains of continuous grain silicon on glass substrate for high-performance TFTs, IEEE Transactions on Electron Devices 51 (2004) 204–211.
[11] N. Yamauchi, J.-J.J. Hajjar, R. Reif, Polysilicon thin-film transistors with channel length and width comparable to or smaller than the grain size of the thin film, IEEE Transactions on Electron Devices 38 (1991) 55–60.
[12] Y. Li, H.-M. Lu, T.-W. Tang, S.M. Sze, A novel parallel adaptive Monte Carlo method for nonlinear Poisson equation in semiconductor devices, Mathematics and Computers in Simulation 62 (2003) 413–420.
[13] Y. Li, S.M. Sze, T.-S. Chao, A practical implementation of parallel dynamic load balancing for adaptive computing in VLSI device simulation, Engineering with Computers 18 (2002) 124–137.
[14] Y. Li, T.-S. Chao, S.M. Sze, A domain partition approach to parallel adaptive simulation of dynamic threshold voltage MOSFET, Computer Physics Communications 147 (2002) 697–701.
[15] Y. Li, J.-L. Liu, T.-S. Chao, S.M. Sze, A new parallel adaptive finite volume method for the numerical simulation of semiconductor devices, Computer Physics Communications 142 (2001) 285–289.
[16] Y. Li, S.-M. Yu, A parallel adaptive finite volume method for nanoscale double-gate MOSFETs simulation, Journal of Computational and Applied Mathematics 175 (2005) 87–99.
[17] Y. Li, S.-M. Yu, A two-dimensional quantum transport simulation of nanoscale double-gate MOSFET's using parallel adaptive technique, IEICE Transactions on Information and Systems E87-D (2004) 1751–1758.
[18] D.L. Scharfetter, H.K. Gummel, Large-signal analysis of a silicon read diode oscillator, IEEE Transactions on Electron Devices ED-16 (1969) 66–77.
[19] T. Kerkhoven, A Proof of Convergence of Gummel's Algorithm for Realistic Device Gemotries, SIAM Journal on Numerical Analysis 23 (1986) 1121–1137.
[20] G.H. Wang, J.M. Tyler, J.S. Weltman, J.D. Callahan, Node-based dynamic adaptive grid with quadrilateral and hexahedral elements, Advances in Engineering Software 30 (1999) 31–41.
[21] D.J. Morton, J.M. Tyler, J.R. Dorroh, A new 3D finite element for adaptive h-refinement in 1-irregular meshes, International Journal for Numerical Methods in Engineering 38 (1995) 3989–4008.
[22] M. Svard, J. Nordstrom, Stability of finite volume approximations for the Laplacian operator on quadrilateral and triangular grids, Applied Numerical Mathematics 51 (2004) 101–125.
[23] M. Stynes, Finite volume methods for convection-diffusion problems, Journal of Computational and Applied Mathematics 63 (1995) 83–90.
[24] Y. Li, A parallel monotone iterative method for the numerical solution of multidimensional semiconductor Poisson equation, Computer Physics Communications 153 (2003) 359–372.
[25] S. Heikkila, V. Lakshmikantham, Monotone Iterative Techniques for Discontinuous Nonlinear Differential Equations, Marcel Dekker, New York, 1994.
[26] C.V. Pao, Accelerated monotone iterations for numerical solutions of nonlinear elliptic boundary value problems, Computers and Mathematics with Applications 46 (2003) 1535–1544.
[27] R.S. Varga, Matrix Iterative Analysis, Springer-Verlag, New York, 2000.